International Journal of Nanomedicine

Dovepress
Taylor & Francis Group

Open Access Full Text Article

ORIGINAL RESEARCH

Reduction-Responsive Nanoparticles Self-Assembled from Sericin-ss-Doxorubicin Conjugate for Hydrophobic IR780 Delivery with Integration of Antitumor Chemo-Phototherapy

Lulu Zhang[1], Haiyang Liu[1], Jin Ren[2], Junyi Shao[1], Yanrong Cao[1], Shuangshuang Wang[1], Changchun Peng[3], Shengwen Shao[1,2], Haixia Ge[1], Jingmou Yu[1,2]

[1]Huzhou Key Laboratory of Medical and Environmental Applications Technologies, School of Life Sciences, Huzhou University, Huzhou, People's Republic of China; [2]Jiangxi Provincial Key Laboratory of Cell Precision Therapy, School of Basic Medical Sciences, Jiujiang University, Jiujiang, 332005, People's Republic of China; [3]Jiangxi Jimin Kexin Pharmaceutical Co., Ltd., Yichun, 332000, People's Republic of China

Correspondence: Haixia Ge; Jingmou Yu, Email ghxzwx2012@163.com; yjm1016@hotmail.com

Background: Stimuli-responsive polymer-drug nanoparticles have emerged as a versatile and effective platform for delivering drugs in the treatment of malignant tumors. The integration of chemo-phototherapy has gained increasing prominence due to its remarkable synergistic antitumor effects.

Methods: Hydrophilic sericin (Ser) was linked to antitumor drug doxorubicin (DOX) via a disulfide bond. The obtained Ser-ss-DOX conjugate was characterized by Fourier-transform infrared spectroscopy (FTIR), proton nuclear magnetic resonance (^{1}H NMR) and dynamic light scattering (DLS). The near-infrared (NIR) fluorescent dye IR780 was encapsulated into Ser-ss-DOX by a dialysis method. The physical state of IR780 within Ser-ss-DOX/IR780 nanoparticles was analyzed by differential scanning calorimetry (DSC). The photothermal properties and drug release behavior of IR780-loaded nanoparticles were systematically investigated. Cellular uptake and reactive oxygen species (ROS) generation capacity and in vitro cytotoxicity of IR780-containing nanoparticles were studied in 4T1 breast cancer cells. In addition, 3D multicellular tumor spheroid model was conducted to investigate the antitumor activity of the nanoparticles.

Results: The Ser-ss-DOX conjugate was successfully synthesized. Ser-ss-DOX and Ser-ss-DOX/IR780 nanoparticles were spherical in shape, and their particle sizes measured by DLS were 326 and 190 nm, respectively. IR780 was in an amorphous state within the Ser-ss-DOX/IR780 nanoparticles. The loading contents of DOX and IR780 were 8.26% and 2.78%, respectively. Ser-ss-DOX/IR780 exhibited ideal photothermal properties in vitro and reduction-sensitive drug release in a high glutathione (GSH) environment. Ser-ss-DOX/IR780 displayed higher cellular uptake in 4T1 cells than Ser-ss-DOX and free DOX. Under 808 nm laser irradiation, Ser-ss-DOX/IR780 showed a strong capacity to generate ROS. Importantly, Ser-ss-DOX/IR780 with laser irradiation effectively inhibited the growth of 4T1 cells and 3D multicellular tumor spheroids.

Conclusion: This work demonstrated that Ser-ss-DOX/IR780 integrated dual functionalities of chemotherapy and phototherapy, thereby enabling substantial potential for application in tumor treatment.

Keywords: polymeric nanoparticles, doxorubicin, sericin, IR780, chemo-phototherapy

Introduction

Cancer is a critical public health problem and ranks as the second leading cause of death worldwide.[1] Traditional treatment modalities, such as chemotherapy and radiotherapy, have been effective in inhibiting cancer progression. However, they are often accompanied by severe side effects.[2] In recent years, polymeric nanoparticles have demonstrated remarkable potential as a safe and effective emerging drug delivery system in cancer therapy.[3] Polymeric nanoparticles,

Received: 13 July 2025
Accepted: 3 November 2025
Published: 11 November 2025

Graphical Abstract

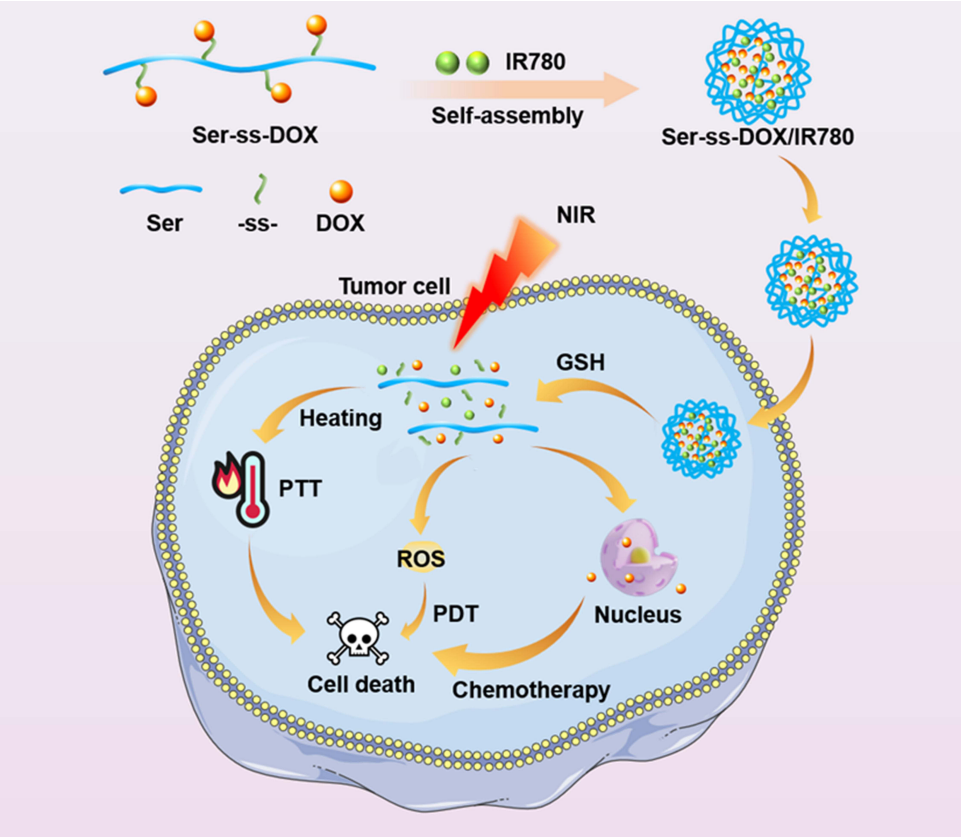

as engineered nanostructures, have been widely applied in drug delivery due to structural versatility for controlled drug release, high kinetic stability, surface functionalization, and ability to protect drugs from environmental degradation.[4]

Amphiphilic copolymers are widely regarded as efficient delivery vehicles for hydrophobic drugs, capable of forming self-assembled nanoparticles in aqueous media with a hydrophilic surface and a hydrophobic core.[5] The shell controls the pharmacokinetic properties of the nanoparticles in the body, while the core can encapsulate insoluble drugs.[6,7] These nanoparticles can significantly enhance the water solubility and bioavailability of hydrophobic drugs. Additionally, polymeric nanoparticles could enable their passive targeting, and augment drug accumulation in tumor sites via the enhanced permeability and retention (EPR) effect.[5]

Recently, stimulus-responsive nanoparticles have attracted growing attention in tumor therapy due to their ability to respond to specific cues within the tumor microenvironment (TME).[8] By enabling targeted and controlled drug delivery, these smart nanoparticles offer significant potential for enhancing therapeutic efficacy and advancing clinical applications.[9] It has been reported that the microenvironment of tumor tissue differs significantly from that of normal physiological tissue. For instance, the concentration of the reducing substance GSH is approximately 2–20 μM in physiological body fluids and normal extracellular matrix, and 1–10 mM in the cytosol of tissue cells. In contrast, its concentration in tumor tissue is 7–10 times higher than in normal tissue.[10] Disulfide bonds can respond to the overexpression of GSH in tumors. Importantly, high concentrations of GSH can be used to selectively disrupt the disulfide bonds of the polymeric nanoparticles, thus achieving targeted drug release.[11] Huang et al developed reduction-responsive mPEG@PCA-g-PCL micelles containing disulfide bonds for paclitaxel delivery. Under normal conditions, the leakage of paclitaxel was limited to less than 30%, whereas nearly all of the drug was released in the reduction media with 40 mM dithiothreitol for 9 h.[12]

The selection of hydrophilic and hydrophobic groups is a critical consideration in the design of polymeric nanoparticles. Sericin (Ser), a protein derived from silkworm cocoons, exhibits excellent hydrophilicity, biocompatibility, low immunogenicity, and biodegradability.[13] Owing to these properties, Ser-based nanoparticles have been extensively explored in drug delivery systems.[14,15] Hu et al previously introduced chitosan into Ser to prepare Ser-based nanoparticles with surface charge reversal properties and encapsulated chemotherapeutic drugs within the nanoparticles.[16] The results demonstrated that Ser had significant potential as a drug delivery material. Doxorubicin (DOX) is a widely used anthracycline antibiotic in current clinical anticancer treatment. It is recognized for its potent cytotoxic activities, which are primarily exerted through the intercalation into DNA, thereby disrupting DNA replication and transcription processes. This ultimately leads to cell apoptosis and inhibition of tumor growth.[17,18] However, DOX-induced cardiotoxicity severely affects the quality of life of patients, limiting its use in the treatment of malignant tumors.[19,20] Presently, nanoparticles formed by coupling a polymer to DOX have been reported for tumor therapy. Huang et al covalently linked Ser to DOX to form sericin-DOX nanoconjugates, and then covalently grafted folic acid onto the conjugates for actively targeting tumor cells.[21] However, folate receptor expression on some normal cells may lead to the uptake of nanoparticles by non-target tissues. As we know, Ser-linked DOX nanoparticles with reduction-sensitivity have not been reported. Herein, disulfide bonds were introduced to synthesize Ser and DOX. Then Ser-ss-DOX conjugate was used to deliver DOX in effective tumor therapy.

Currently, combinational therapy has gained increasing attraction, due to its ability to enhance therapeutic efficacy and reduce drug resistance.[22] Chemo-phototherapy synergism has emerged as a potent therapeutic strategy with substantial potential for tumor treatment.[23,24] Phototherapy is usually categorized into photothermal therapy (PTT) and photodynamic therapy (PDT). PTT utilizes light energy to generate heat via photothermal agents, thereby inducing cellular damage. It boasts advantages such as non-invasiveness, low toxicity, and reduced susceptibility to drug resistance, while demonstrating encouraging therapeutic efficacy in precision tumor treatment.[25] PDT employs light-activated photosensitizers to selectively produce cytotoxic reactive oxygen species (ROS) within tumor tissues, thereby enabling localized oxidative damage and tumor cell death.[26] IR780 is a lipophilic small-molecule cyanine dye with strong light absorption and emission capabilities in the near-infrared (NIR) region and is often used as a photothermal agent and photosensitizer in the treatment of cancer.[24,27] This small molecule has an absorption peak at 780 nm. Under NIR irradiation, IR780 can effectively raise the temperature and generate ROS to induce tumor cell damage.[28] Compared with indocyanine green, IR780 exhibits superior photostability and fluorescence imaging performance, thereby endowing IR780-based therapies with greater potential for application in tumor treatment.[29,30] However, IR780 is water-insoluble, and it cannot be administered by intravenous injection with high bioavailability.[31] Further, the injected IR780 was eliminated quickly in vivo.[27] And IR780 administered via injection with a high dose (>1 mg/kg) could induce acute toxicity in mice.[27] To enhance the water solubility of IR780, prolong its retention time within tumors, suppress its toxicity, and promote its accumulation in cancer cells, IR780 could be encapsulated within the hydrophobic core of polymeric nanoparticles, thereby overcoming its inherent limitations.[32]

In this work, a Ser-based nanoplatform with reductive sensitivity containing DOX and IR780 is designed for tumor therapy. Ser was selected as the hydrophilic backbone, and DOX was conjugated to Ser via a reduction-responsive disulfide bond to synthesize the amphiphilic Ser-ss-DOX. IR780 was encapsulated into the self-assembled nanoparticles, resulting in the preparation of Ser-ss-DOX/IR780 nanoparticles. The Ser-ss-DOX/IR780 nanoparticles were characterized, and their reduction-responsive drug release and photothermal properties were investigated. The cellular uptake, ROS generation, cytotoxicity, and cell penetration effects of the IR780-loaded nanoparticles were evaluated in 4T1 breast cancer cells.

Materials and Methods

Materials

Ser, 4-dimethylaminopyridine (DMAP), GSH, pyrene, *N*-(3-dimethylaminopropyl)-*N*′-ethylcarbodiimide hydrochloride (EDC), *N*-hydroxy succinimide (NHS), IR780, 2′,7′-dichlorodihydrofluorescein diacetate (DCFH-DA), and 3-(4,5-dimethyl-2-thiazolyl)-2,5-diphenyl-2H-tetrazolium bromide (MTT) were provided by Aladdin Industrial Corporation (Shanghai, China). DOX·HCl was purchased from Beijing Huafeng United Technology Co. Ltd (Beijing, China). *N, N*′-dicyclohexylcarbodiimide (DCC), Hoechst 33342 and 3,3′-dithiodipropionic acid (DPA) were bought from Sigma-Aldrich (St. Louis, OM, USA). Anti-

fluorescence quenching sealing solution, paraformaldehyde, and 3D Cell Culture Envelope Kit were purchased from Beyotime (Shanghai, China). RPMI 1640 medium and Trypsin were purchased from Zhejiang Senrui Biotechnology Co. Ltd. (Huzhou, China). Fetal bovine serum (FBS) was from Zhejiang Tianhang Biotechnology Co. Ltd. (Huzhou, China).

4T1 cells were provided by the China Center for Type Culture Collection (Wuhan, China). The culture environment is 37 °C, and the incubator contains 5% CO_2. The cells were cultured in RPMI-1640 media containing 10% fetal bovine serum and 1% penicillin-streptomycin.

Synthesis of Ser-Ss-DOX Polymer

Ser was conjugated with DOX in two steps, as shown in Figure 1A. First, Ser (1.0 g) was dispersed in 20 mL of deionized water and 30 mL of dimethyl sulfoxide (DMSO). DPA (200 mg), EDC (377 mg) and NHS (219 mg) were completely dissolved in 30 mL of DMSO and 20 mL of deionized water. The above solutions were mixed and stirred in the dark for 24 h at room temperature. Subsequently, the mixture was dialyzed against deionized water. After dialysis, the solution is lyophilized to obtain DPA-modified Ser (Ser-DPA) conjugate.

In the second step, Ser-DPA (50 mg) was dissolved in 25 mL deionized water. DOX (10 mg), triethylamine (7.2 μL), DMAP (4.2 mg) and DCC (7.1 mg) were dissolved in 25 mL ethanol. The two solutions described above were mixed and then stirred for 24 h in the dark. Next, the mixed solution was dialyzed with deionized water and then freeze-dried to obtain Ser-ss-DOX. The chemical structure of the conjugates was verified by Fourier transform infrared (FTIR) (Bruker

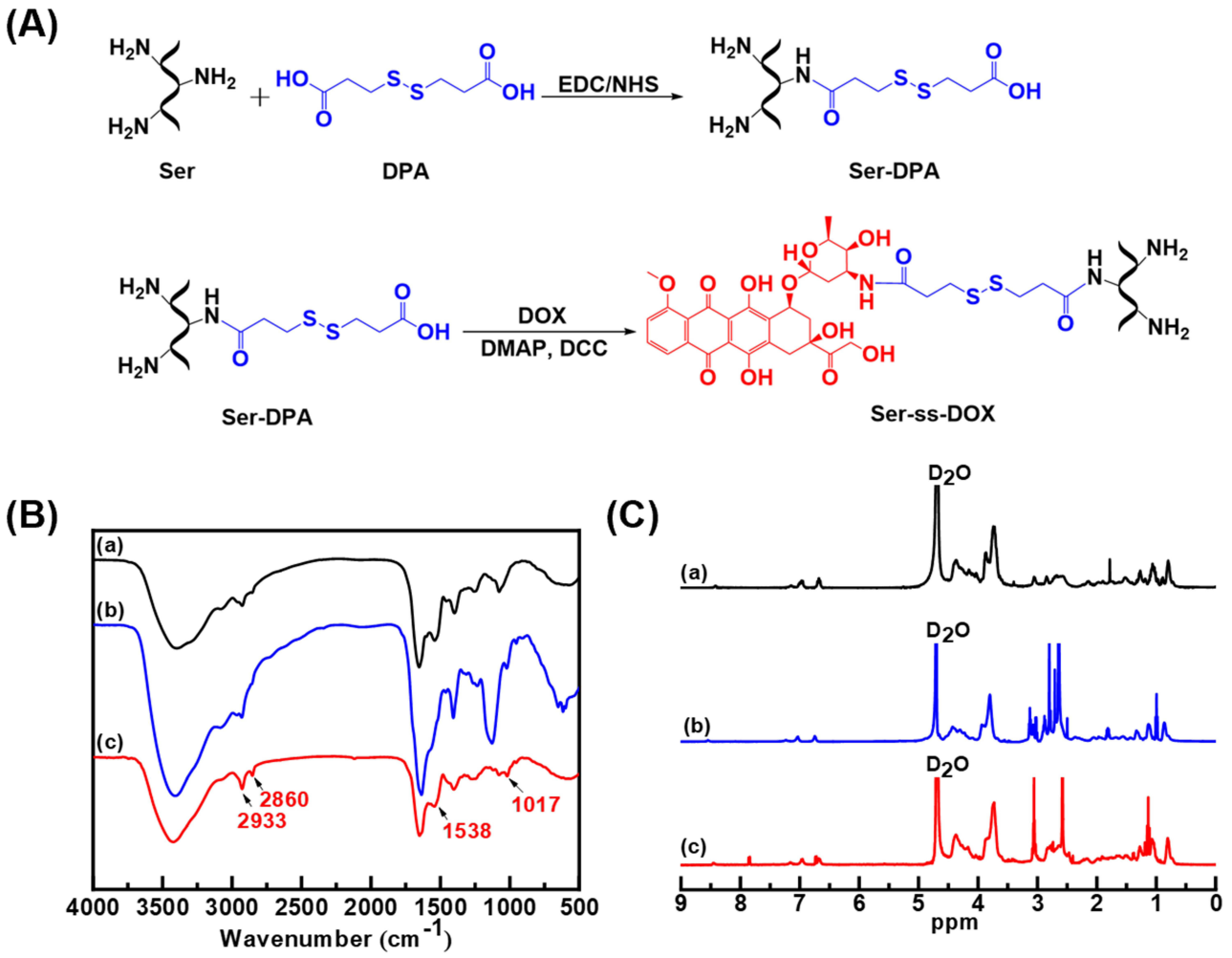

Figure 1 (**A**) Synthesis pathway of Ser-ss-DOX conjugate. (**B**) FTIR spectra of (a) Ser, (b) Ser-DPA and (c) Ser-ss-DOX. (**C**) ^{1}H NMR spectra of (a) Ser, (b) Ser-DPA and (c) Ser-ss-DOX.

Tensor II, Germany) and ^{1}H NMR (Avance DMX500, Bruker, Germany). The content of DOX in Ser-ss-DOX was investigated by a UV-Vis spectrophotometer with the detection wavelength at 481 nm.

Preparation of IR780-Loaded Nanoparticles

IR780 was encapsulated into nanoparticles through the dialysis process.[33] Briefly, Ser-ss-DOX (40 mg) was dissolved in a mixture of DMSO and deionized water. An 8 mg amount of IR780 was dissolved in 8 mL DMSO and gradually introduced into the Ser-ss-DOX nanosuspension, followed by stirring for 48 h at ambient temperature under dark conditions. Then the mixture was dialyzed with deionized water for 24 h. The dialysis solution was freeze-dried, and finally Ser-ss-DOX/IR780 was obtained.

Characterization of the Nanoparticles

The shape of the nanoparticles was detected by transmission electron microscopy (TEM) (JEM-1230, Jeol, Japan). The mean diameter and zeta potential of Ser-ss-DOX and Ser-ss-DOX/IR780 nanoparticles were analyzed by DLS (90Plus, Brookhaven Instruments Corp., USA). To evaluate the stability of Ser-ss-DOX/IR780, the size changes of the nanoparticles were measured in deionized water, PBS or GSH-containing aqueous media.

The loading content (LC) of IR780 in the nanoparticles was determined by an ultraviolet-visible spectrophotometer. IR780-loaded self-assembled nanoparticles were dissolved in DMSO and the amount of IR780 was measured at 780 nm. The calculated formula was LC = (amount of IR780 loaded in nanoparticles/amount of IR780-containing nanoparticles) × 100%.

The state of IR780 within the Ser-ss-DOX/IR780 nanoparticles was examined using DSC (Discovery DSC 25, TA Instruments, USA). The scanning temperature ranged from 30 °C to 280 °C, increasing at a rate of 10 °C per minute. Thermal spectra of Ser-ss-DOX/IR780, Ser-ss-DOX and IR780 were investigated.

The release profile of Ser-ss-DOX/IR780 nanoparticles was studied by using the dialysis method. The IR780-loaded nanoparticles (1 mL) were encapsulated in a dialysis bag and immersed in a tube containing 20 mL of release medium. The release medium was phosphate buffer solution (PBS, pH 7.4) or PBS containing 20 mM GSH. The tubes were placed on a shaker at 37 °C. All release media were removed at predetermined time intervals, followed by the addition of an equal volume of fresh-release media. The release amounts of DOX were measured by using a fluorescence spectrophotometer (Hitachi F-7000, Japan).

Photothermal Performance

The photothermal properties of IR780-loaded nanoparticles were evaluated by monitoring the temperature changes within 5 min of laser irradiation. Ser-ss-DOX/IR780 was dissolved in water at different concentrations. IR780 was dissolved in DMSO to prepare solutions at the same corresponding concentrations. Water, DMSO, and DOX·HCl were measured under the same conditions. A semiconductor laser device (Changchun Leishi Photo-Electric Technology Co., Ltd., China) was used to irradiate the solution at 2 W/cm^2 under an 808 nm laser. The temperature of different solutions was photographed and recorded by a thermal imaging camera (Hikvision, H10, Hangzhou, China) at a predetermined time.

In vitro Cellular Uptake

The cellular uptake of Ser-ss-DOX/IR780 nanoparticles was investigated in 4T1 cells. Briefly, the cells were plated at a density of 6×10^4 into a glass-bottomed petri dish with a diameter of 35 mm, and placed in a CO_2 incubator for 72 h. After the cells were completely adhered to the culture dish, the original medium was replaced with fresh medium containing Ser-ss-DOX/IR780, Ser-ss-DOX or DOX·HCl, respectively. The cells were then cultured for an additional 4 h. Then the drug-containing media were removed, and fresh medium was introduced. Some cells were irradiated using an 808 nm laser (2.0 W/cm^2) for 3 min. After a 1 h incubation period, the cells underwent triple washing with PBS. Fluorescent signals in the cells were captured by using inverted fluorescence microscopy (Olympus IX73, Japan).

Assessment of ROS Generation

ROS formation in 4T1 cells was detected by using DCFH-DA as a fluorescent probe.[34] To evaluate the generation of ROS in Ser-ss-DOX/IR780 nanoparticles, 4T1 cells were seeded at a density of 6×10^4 into 35 mm glass-bottom dishes.

As cell attachment was complete, the culture medium was discarded. The cells were co-cultured with Ser-ss-DOX/IR780, Ser-ss-DOX or DOX·HCl for 4 h, respectively. Subsequently, the cells were washed with PBS and replenished with fresh culture media. Some cells were subjected to 808 nm laser exposure (2.0 W/cm^2) for 3 min, followed by 1 h incubation. The original media were replaced by adding 40 μM DCFH-DA, and the cells were co-incubated for 2 h. Afterwards, the cells were washed with PBS and stained with Hoechst 33342 (10 μg/mL) for 30 min. The media were replaced with PBS. Cellular fluorescence was monitored by fluorescence microscopy.

In vitro Cytotoxicity

The cytotoxic effects of drug-containing nanoparticles were evaluated in 4T1 cells by the MTT assay.[35] The cells were inoculated into 96-well plates at 1×10^4 cells per well and incubated for 24 h. The original medium was discarded, and the cells were incubated with fresh medium containing various concentrations of Ser-ss-DOX/IR780, Ser-ss-DOX, DOX·HCl, IR780, or DOX + IR780 for 4 h. Then the media were discarded. Some cells were irradiated with 808 nm laser (2 W/cm^2, 3 min). All cells were incubated for 20 h. The original media were replaced with 130 μL of MTT solution. After 4 h, the solution was removed and 130 μL DMSO was added. Fifteen minutes later, absorbance was recorded at 490 nm by using a microplate reader.

In order to clearly describe the degree of synergy between DOX and IR780, the combination index (CI) was calculated by using the formula CI = $(C)_1/(Dx)_1 + (C)_2/(Dx)_2$. Here, $(C)_1$ and $(C)_2$ represent the concentrations of each drug in combination that achieve a certain effect of growth inhibition (Fa, the fraction affected by a particular dose), while $(Dx)_1$ and $(Dx)_2$ are the concentrations needed for each drug alone to produce the same effect. The CI analysis was conducted according to the method of Chou and Talalay using CompuSyn software.[36] Synergistic, additive, and antagonistic effects are defined by CI values of <1, =1, and >1, respectively.[37]

Penetration of 3D Multicellular Tumor Spheroids

A three dimensional (3D) multicellular tumor spheroid model was utilized to mimic solid tumors.[38] The antitumor efficacy of Ser-ss-DOX/IR780 nanoparticles was further evaluated. U-shaped 96-well plates were pretreated by using the 3D Cell Culture Envelope Kit. 4T1 cells were seeded at a density of 1×10^4 cells per well to establish a 3D tumor spheroid model. 3D tumor spheroids with near-uniform size were employed to investigate the penetration ability of Ser-ss-DOX/IR780, Ser-ss-DOX, DOX·HCl, IR780 and DOX + IR780. After 8 h of drug administration, some cells were irradiated using a laser (2 W/cm^2, 3 min). The extent of tumor ablation was assessed by fluorescence microscopy. Image J software was utilized to assess the changes in the diameter of 3D tumor spheroids before and after treatment, providing insights into the tumor volume ablation capability of drug-containing nanoparticles.

Statistical Analysis

The data were expressed as mean ± standard deviation (SD). One-way ANOVA with a Bonferroni post-hoc test was employed to compare mean values across three or more groups, while a two-sample *t*-test was adopted for comparisons between two groups. Differences were considered statistically significant at $*p < 0.05$, $**p < 0.01$, $***p < 0.001$.

Results and Discussion

Synthesis and Characterization of Ser-Ss-DOX

Ser-ss-DOX conjugate was synthesized by connecting Ser and DOX through reduction-responsive disulfide bonds, and the synthesis process was shown in Figure 1A. Briefly, Ser-ss-DOX was synthesized by a two-step process. Ser-DPA was first synthesized through an amidation reaction between Ser and DPA, which contains an internal disulfide bond. Subsequently, the obtained Ser-DPA and hydrophobic DOX were conjugated to synthesize Ser-ss-DOX. The antitumor drug DOX exhibited potent antitumor activity, and Ser demonstrated good biocompatibility with minimal immunogenic responses.[39] In addition, water, ethanol and DMSO were utilized as solvents in the synthesis of Ser-ss-DOX. Owing to the favorable properties of these solvents, such as their ready availability and eco-friendliness, the synthesis is well-suited for mass production.

Further, the synthesized conjugate was verified by FTIR and ^{1}H NMR. As shown in Figure 1B, Ser, Ser-DPA and Ser-ss-DOX exhibited distinct characteristic peaks around 2933 cm^{-1}, corresponding to the C–H stretching vibrations. This observation confirms the presence of Ser in the synthesized conjugate.[40] Compared to Ser, the peaks at 1017 cm^{-1} (ester group) in Ser-DPA significantly increased.[41] Ser-ss-DOX exhibited a characteristic peak at 1017 and 1538 cm^{-1}, providing evidence for the formation of an amide linkage between Ser-DPA and DOX. To verify the chemical structure of the polymers, ^{1}H NMR analysis was adopted. As shown in Figure 1C, compared with Ser, Ser-DPA has characteristic peaks of DPA at 2.47 to 3.22 ppm. In the spectra of Ser-ss-DOX and Ser-DPA, it was found that the characteristic peaks of DOX appeared at 0.96, 1.23, 2.84 and 7.82 ppm, indicating that DOX had been successfully connected with Ser-DPA. DOX content was quantified as 8.26% by measuring absorbance at 481 nm with a UV-Vis spectrophotometer.

Characterization of the Nanoparticles

The amphiphilic Ser-ss-DOX is capable of self-assembling into micelles in aqueous media, and the CMC value of Ser-ss-DOX can be determined using a pyrene fluorescent probe. As shown in Figure 2A, the CMC value of Ser-ss-DOX was 0.109 mg/mL. These results indicate that Ser-ss-DOX readily forms stable micelles in aqueous environments, making it an effective carrier for hydrophobic drugs. As shown in Figure 2B, Ser-ss-DOX nanosuspension was red, while Ser-ss-DOX/IR780 appeared green. This phenomenon indicated that IR780 was effectively encapsulated into the nanoparticles. The LC of IR780 in Ser-ss-DOX/IR780 was 2.78%. As shown in Figure 2C and D, Ser-ss-DOX and Ser-ss-DOX/IR780 nanoparticles observed by TEM exhibited a spherical morphology. Besides, the size of Ser-ss-DOX was significantly larger than that of Ser-ss-DOX/IR780. The mean diameter of Ser-ss-DOX was 326 nm by DLS analysis (Figure 2E). As IR780 was physically encapsulated into Ser-ss-DOX, the mean diameter decreased at 190 nm. This size reduction may be attributed to the more compact hydrophobic core after IR780 encapsulation. These results were consistent with the TEM results. The polydispersity index (PDI) for Ser-ss-DOX and Ser-ss-DOX/IR780 is 0.214 and 0.208, respectively (Figure 2E). A low PDI indicated a narrow size of these nanoparticles. The zeta potentials of Ser-ss-DOX and Ser-ss-DOX/IR780 were −26.17 and −29.98 mV, respectively (Figure 2F). The negative potential is beneficial for the effective passage of the drug through blood vessels and its accumulation within tumors.[42] Furthermore, the negatively charged surface promotes favorable interactions with the slightly positively charged endothelium of tumor vasculature. Combined

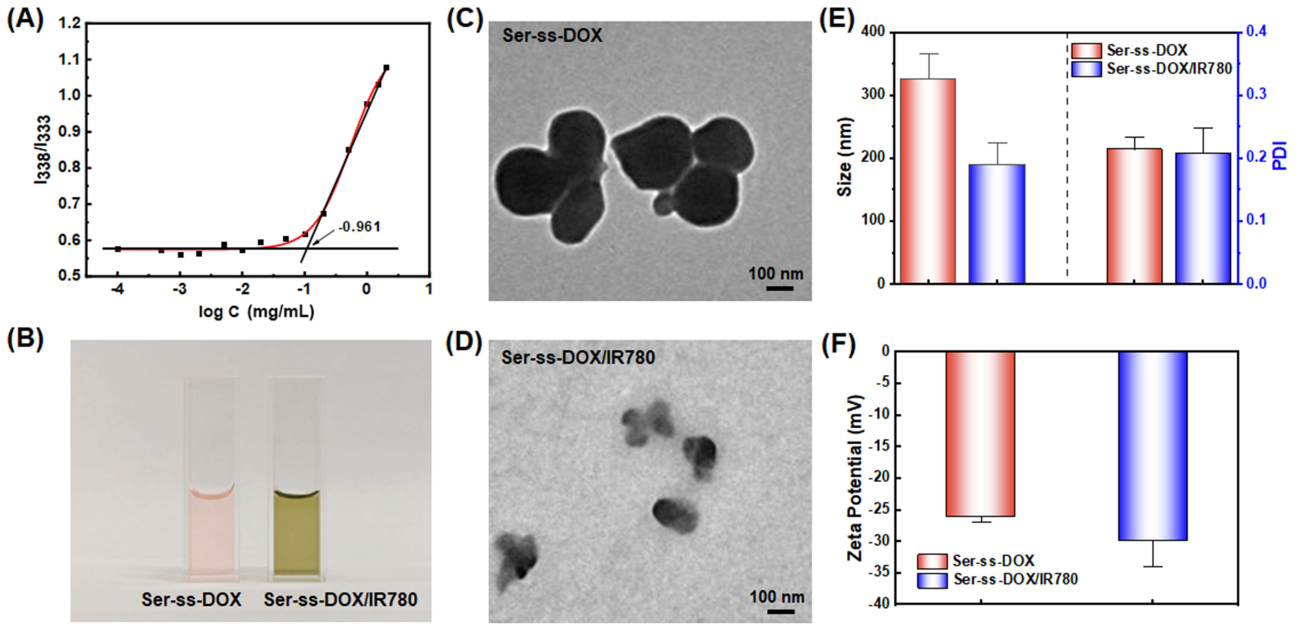

Figure 2 (**A**) Plot of I_{338}/I_{333} ratio vs log C based on pyrene excitation spectra of Ser-ss-DOX, (**B**) Images of Ser-ss-DOX and Ser-ss-DOX/IR780 dispersed in water, (**C** and **D**) TEM images of Ser-ss-DOX and Ser-ss-DOX/IR780. (**E**) Particle size and polydispersity index (PDI) of Ser-ss-DOX and Ser-ss-DOX/IR780. (**F**) Zeta potential of Ser-ss-DOX and Ser-ss-DOX/IR780 nanoparticles.

https://doi.org/10.2147/IJN.S553474

with the EPR effect characteristic of tumor tissues, this facilitates efficient extravasation of the nanoparticles across vascular barriers.

As depicted in Figure 3A, the average size of Ser-ss-DOX/IR780 nanoparticles showed negligible changes within 48 h in deionized water and PBS. These results indicated that Ser-ss-DOX/IR780 nanoparticles had high stability. However, upon exposure to 20 mM GSH, a substantial increase in size was observed in 10 min, leading to the formation of large aggregates at about 1500 nm (Figure 3B). After 30 minutes, the nanoparticle size had increased to nearly 2700 nm. This GSH-induced aggregation validated the reduction-sensitive nature of the nanoparticles. Furthermore, the increase in particle size is likely due to the release of IR780 following nanoparticle decomposition. As IR780 is insoluble in water, it tends to aggregate in aqueous solution.[31]

The physical state of IR780 in the Ser-ss-DOX/IR780 nanoparticles was investigated by using DSC. As shown in Figure 3C, pure IR780 exhibited a distinct endothermic melting peak at 255 °C. However, this peak was absent in Ser-ss-DOX and Ser-ss-DOX/IR780. These results indicated that IR780 was in an amorphous state within the Ser-ss-DOX /IR780 nanoparticles, demonstrating its effective dispersion.

The DOX release behavior of Ser-ss-DOX/IR780 nanoparticles was evaluated by simulating the in vivo environment (37 °C, pH 7.4, with or without 20 mM GSH). As illustrated in Figure 3D, the cumulative release of DOX from Ser-ss-DOX/IR780 in PBS reached approximately 43% over 120 h. Notably, in PBS containing 20 mM GSH, the cumulative

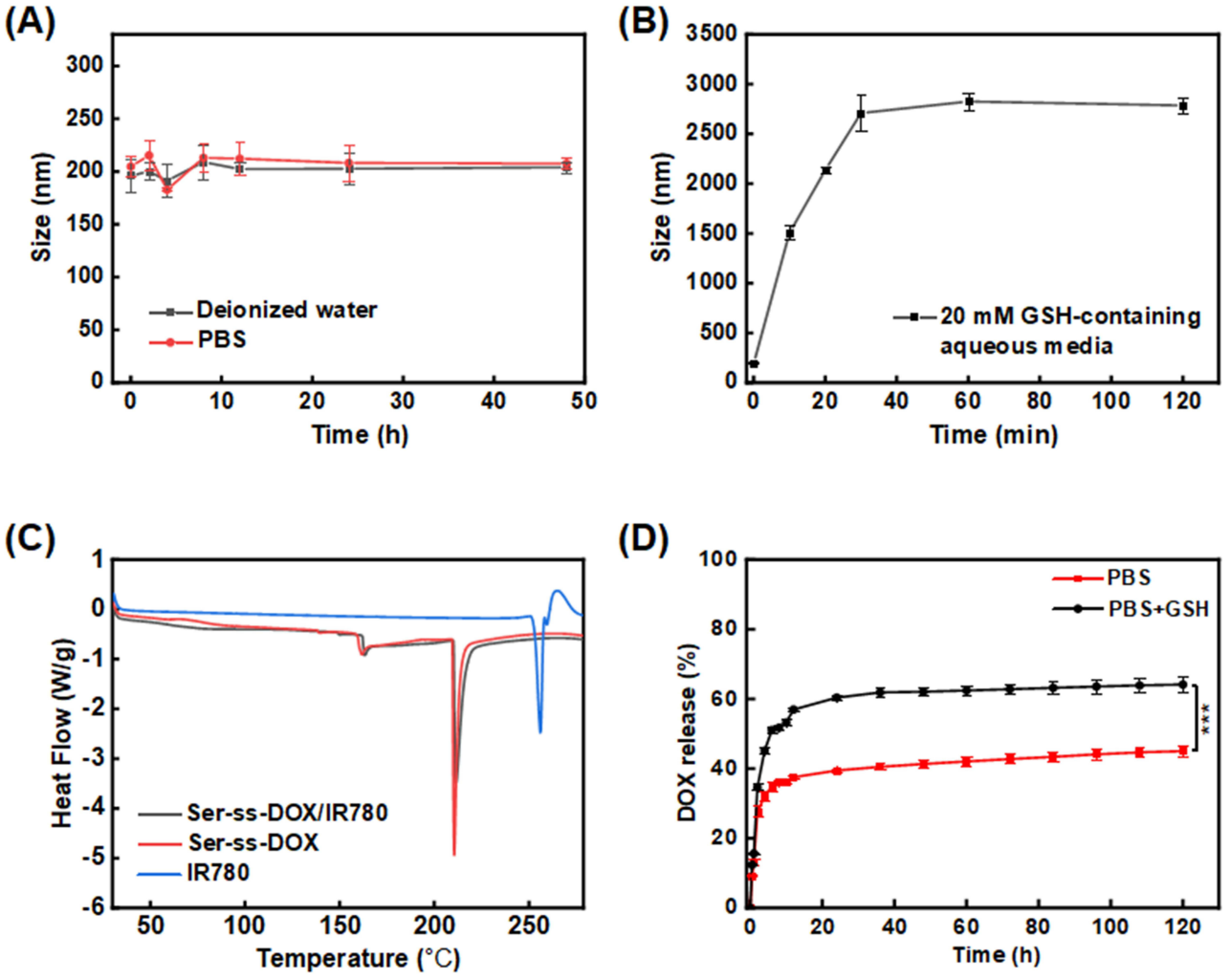

Figure 3 (**A**) Size changes of Ser-ss-DOX/IR780 nanoparticles in deionized water and PBS. (**B**) Size changes of Ser-ss-DOX/IR780 nanoparticles in 20 mM GSH-containing aqueous media. (**C**) DSC spectra of Ser-ss-DOX, Ser-ss-DOX/IR780 and IR780. (**D**) DOX release profiles of Ser-ss-DOX/IR780 in PBS (pH 7.4) with or without 20 mM GSH at 37 °C. (n = 3). ***$P < 0.001$.

release of DOX increased to about 62%, representing a significant enhancement in drug release kinetics. This phenomenon arises from sulfhydryl-disulfide bond exchange reactions triggered by high GSH concentrations, which disrupt disulfide linkages and facilitate the rapid release of DOX.[43] These results demonstrated that Ser-ss-DOX/IR780 had a reduction response, enabling accelerated DOX release in the tumor microenvironment and thereby improving drug bioavailability.

Photothermal Performance

The photothermal performance of IR780 and Ser-ss-DOX/IR780 was evaluated under irradiation with an 808 nm NIR laser. As shown in Figure 4A, IR780 exhibited strong photothermal properties, and the temperature increase was dependent on irradiation time and IR780's concentration. The temperature gradually increases with increasing laser irradiation time. After 5 minutes of laser irradiation, the temperature of a 5 μg/mL IR780 solution increased by 5 °C, while the temperature increases in IR780 solutions at the concentrations of 10 μg/mL, 25 μg/mL, and 50 μg/mL were 11 °C, 18.9 °C, and 23.3 °C, respectively. As depicted in Figure 4B, under identical irradiation conditions, the temperature elevation of Ser-ss-DOX/IR780 nanoparticles was comparable to that of free IR780. These results inferred that Ser-ss-DOX retained the photothermal activity of IR780. Furthermore, negligible temperature changes were observed in the DMSO, DOX·HCl or H_2O groups under laser irradiation, confirming the absence of photothermal effects of these samples. As illustrated in Figure 4C, NIR thermal images revealed the temperature variations among different samples. These results demonstrated that IR780 exhibited ideal photothermal effects, which were preserved upon incorporation into the nanoparticles. Therefore, Ser-ss-DOX/IR780 nanoparticles showed promising potential for PTT in tumor treatment.

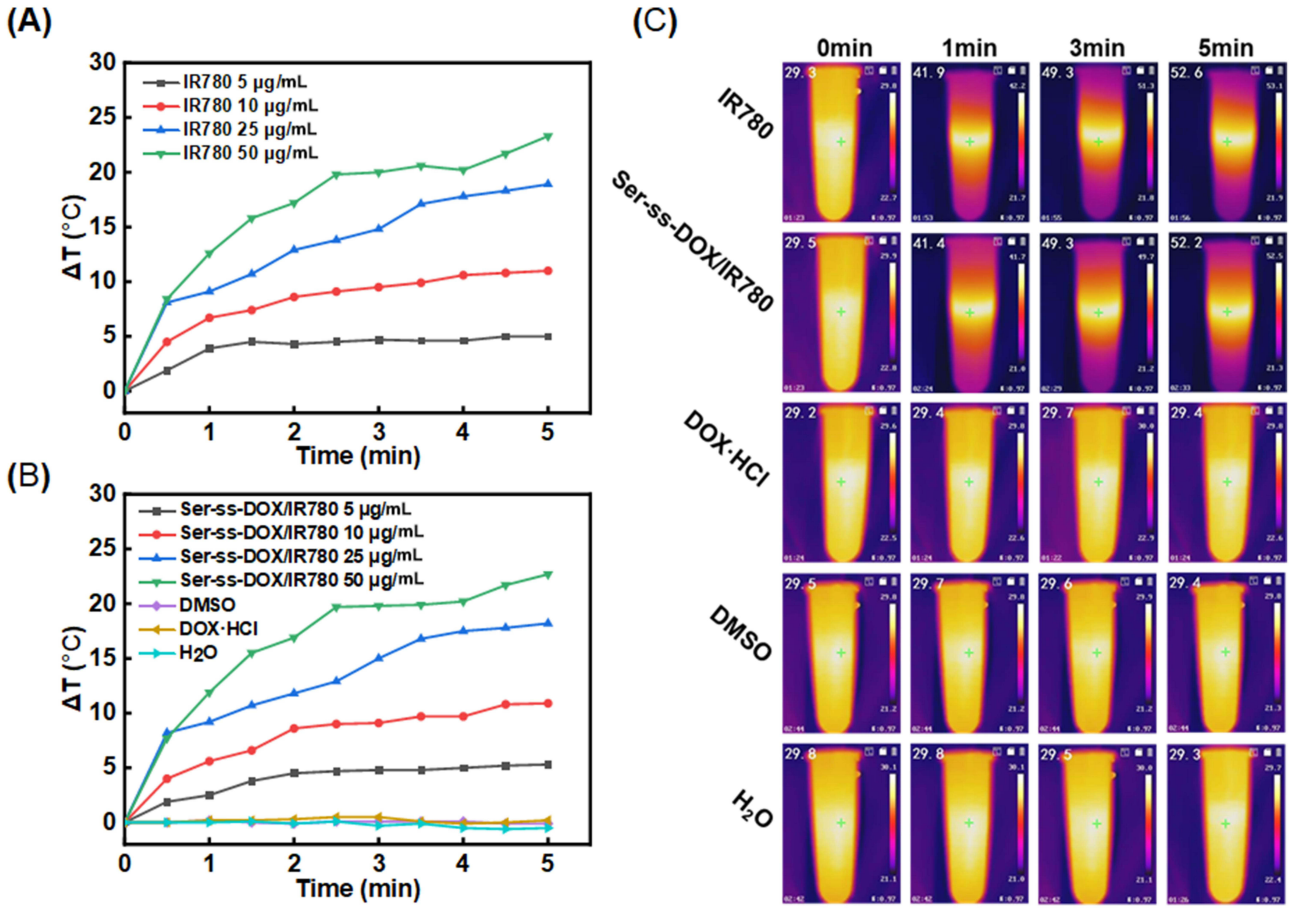

Figure 4 (**A**) Temperature changes of IR780 with different concentrations under NIR irradiation within 5 min. (**B**) Temperature changes of Ser-ss-DOX/IR780, DMSO, DOX·HCl and H_2O within 5 min of NIR irradiation. (**C**) Infrared thermal images of IR780, Ser-ss-DOX/IR780, DOX·HCl, DMSO and H_2O under NIR irradiation within 5 min.

https://doi.org/10.2147/IJN.S553474

In vitro Cellular Uptake

The cellular uptake of Ser-ss-DOX/IR780 nanoparticles in 4T1 cells was observed by fluorescence microscopy. As shown in Figure 5, DOX emitted red fluorescence. Compared with DOX·HCl, Ser-ss-DOX and Ser-ss-DOX/IR780 nanoparticles exhibited stronger red fluorescence. These results were due to the enhanced DOX uptake by the nanoparticles and triggered drug release under the influence of high levels of GSH in tumor cells. Interestingly, the red fluorescence of Ser-ss-DOX/IR780 was enhanced after NIR irradiation. It might be due to the fact that IR780-loaded nanoparticles can produce a local thermal effect after NIR irradiation, which increases the permeability of the cell membrane and effectively enhances cellular uptake of the nanoparticles.[44] The lower fluorescence intensity from DOX·HCl may be attributed to drug cellular uptake by passive diffusion with small quantities.[45] These results suggested that Ser-ss-DOX/IR780 enhanced the permeability capacity of DOX into cells and effectively released the loaded drug.

Assessment of ROS Generation

Under NIR irradiation, IR780 demonstrates a robust capacity to generate ROS, including singlet oxygen and superoxide anions.[46] This characteristic is pivotal in photodynamic therapy (PDT). The generated ROS can trigger oxidative stress, which disrupts cellular components such as lipids, proteins and DNA, leading to cell death through apoptosis or necrosis in tumor tissues. Ser-ss-DOX/IR780, Ser-ss-DOX or DOX·HCl was cultured with 4T1 cells for 4 h to investigate the intracellular ROS production by using DCFH-DA probe. DCFH-DA is initially non-fluorescent. However, upon entering tumor cells, it undergoes hydrolysis and oxidation to form 2′,7′-dichlorofluorescein (DCF), a compound that emits green fluorescence.[47] As illustrated in Figure 6, the green fluorescence was strongest from Ser-ss-DOX/IR780 (NIR), indicating that Ser-ss-DOX/IR780 (NIR) generated a greater amount of ROS. At the same time, there was no significant ROS

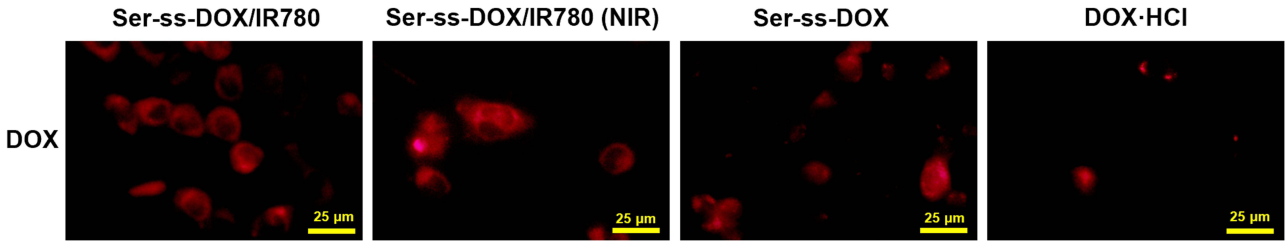

Figure 5 Fluorescence images of 4T1 cells after 4 h of co-incubation with Ser-ss-DOX/IR780 (with or without NIR), Ser-ss-DOX and DOX·HCl.

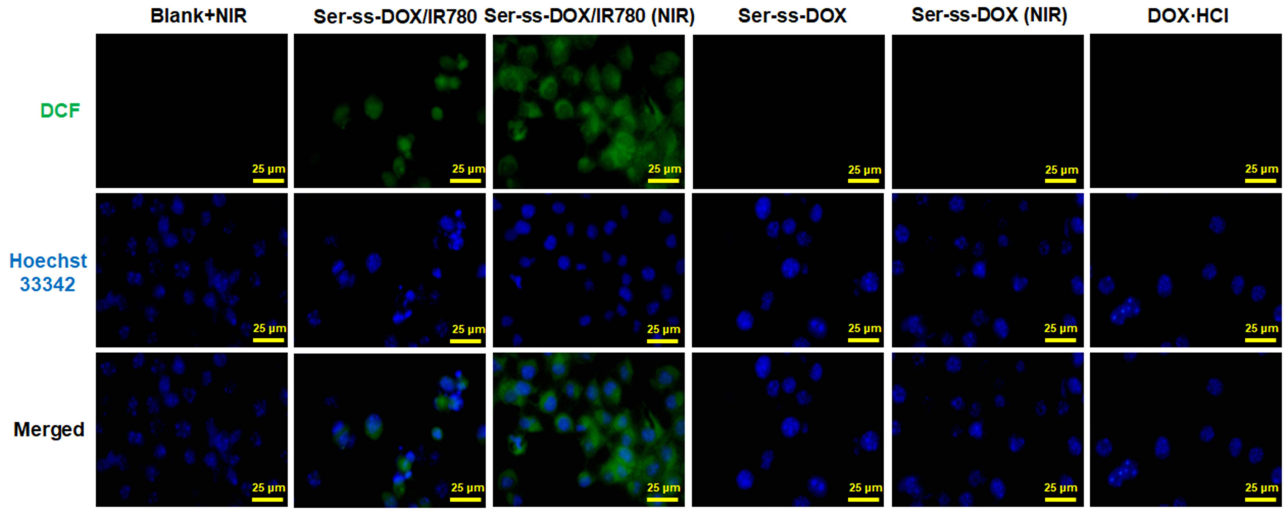

Figure 6 Fluorescence images of intracellular ROS production in 4T1 cells after 4 h co-incubation with blank culture media (NIR), Ser-ss-DOX/IR780 (NIR), Ser-ss-DOX, Ser-ss-DOX (NIR) or DOX·HCl.

production in the blank culture media, Ser-ss-DOX and DOX-HCl groups. The results demonstrated that the generation of ROS was associated with IR780. Upon NIR irradiation, IR780 is capable of producing ROS, leading to cytotoxic effects that can be harnessed for PDT treatment.

In vitro Cytotoxicity

The cytotoxicity of Ser-ss-DOX/IR780 nanoparticles in 4T1 breast cancer cells was assessed using the MTT assay. As illustrated in Figure 7A, all groups showed dose-dependent inhibition of cell growth in the absence of laser exposure. Ser-ss-DOX/IR780 demonstrated stronger cytotoxicity than Ser-ss-DOX and DOX·HCl. Meanwhile, the cytotoxicity of DOX·HCl was slightly lower than that of Ser-ss-DOX, suggesting that drug-loaded nanoparticles could improve intracellular DOX delivery into 4T1 cells. As shown in Figure 7B, under NIR irradiation, all groups exhibited dose-dependent cytotoxicity toward 4T1 cells. At the same concentration, Ser-ss-DOX/IR780 under laser irradiation demonstrated the strongest inhibition of cell activity among all groups. At a DOX concentration of 8 μg/mL, Ser-ss-DOX/IR780 (NIR) treatment resulted in a cell survival rate of only 10.26%, significantly lower than the 27.96% of Ser-ss-DOX/IR780 ($P < 0.01$). In addition, DOX + IR780 (NIR) exhibited stronger cell inhibition than IR780 (NIR) or DOX·HCl. The results above demonstrate that Ser-ss-DOX/IR780 can effectively deliver drugs to cancer cells and promote reduction-responsive drug release, thereby achieving synergistic effects between chemotherapy and phototherapy. This approach exhibits excellent therapeutic efficacy and possesses certain clinical translation potential.

To further describe the synergistic chemo-phototherapy, the CI values were calculated. As shown in Figure 7C, CI values (0.715, 0.566, 0.706 and 0.696) were less than 1. These results indicated that DOX+IR780 combination in Ser-ss-DOX/IR780 nanoparticles (NIR) exhibited desirable synergistic cytotoxicity against 4T1 cells. Chemotherapy and radiotherapy are the current mainstays for breast cancer treatment. However, chemotherapy is limited by its lack of specificity and severe side effects, while radiotherapy is frequently associated with toxicity. Therefore, the reduction-responsive Ser-ss-DOX/IR780 offers a promising chemo-phototherapeutic approach with strong clinical prospects.

Penetration of 3D Multicellular Tumor Spheroids

In contrast to monolayer cells, 3D multicellular tumor spheroid models more accurately recapitulate the microenvironment of solid tumors, and drugs screened by the 3D models may possess greater clinical research values.[48,49] The antitumor effects of drug-loaded nanoparticles were further evaluated in 3D tumor spheroids of 4T1 cells. In Figure 8A, the morphological changes of the 3D tumor spheroids were presented by different sample treatments at 0 h and 8 h with or without NIR. After 8 h of treatment with different formulations, some spheroids were irradiated with a laser (2 W/cm^2, 3 min). The volume reduction ratios of 4T1 cell spheroids are presented in Figure 8B, and these observations correlate well with in vitro cytotoxicity results. Among all treatment groups, the Ser-ss-DOX/IR780 (NIR) group demonstrated the highest percentage reduction in tumor spheroid volume, reaching 16.34%. This reduction was significantly greater than the 14.93% observed in the Ser-ss-DOX/IR780 group ($P < 0.05$), indicating that Ser-ss-DOX/IR780 (NIR) could effectively mediate tumor cell killing upon laser irradiation. Additionally, compared with the 11.09% reduction observed

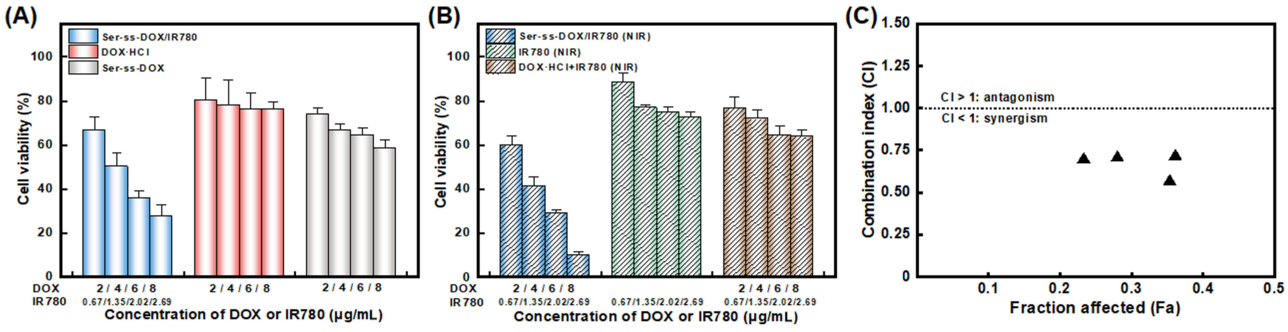

Figure 7 In vitro evaluation of the cytotoxicity of various formulations on 4T1 cells, without (**A**) and with (**B**) 808 nm NIR laser treatment (n = 3). (**C**) Combination index of DOX and IR780 in Ser-ss-DOX/IR780 nanoparticles (NIR) against 4T1 cells.

https://doi.org/10.2147/IJN.S553474

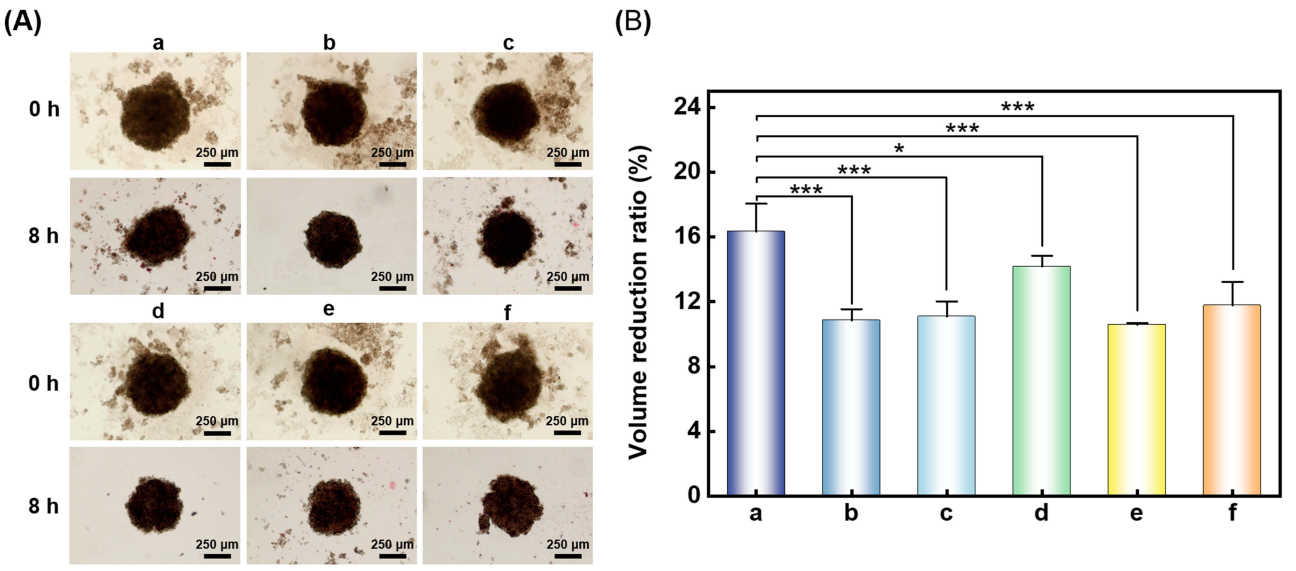

Figure 8 (**A**) Images and (**B**) volume reduction ratio of 4T1 cell spheroids with the treatment of different formulations in the presence or absence of NIR irradiation. (a) Ser-ss-DOX/IR780 (NIR), (b) IR780 (NIR), (c) DOX + IR780 (NIR), (d) Ser-ss-DOX/IR780, (e) DOX·HCl, (f) Ser-ss-DOX. (n = 3). *P < 0.05, ***P < 0.001.

in the DOX·HCl + IR780 (NIR) group, Ser-ss-DOX/IR780 displayed a stronger tumor spheroid-killing capacity after laser irradiation (P < 0.001). Furthermore, the percentage reduction in tumor spheroid volume for Ser-ss-DOX was significantly lower than that for Ser-ss-DOX/IR780 (NIR) (P < 0.001), indicating that IR780-containing nanocarriers exert a phototherapeutic effect. Therefore, Ser-ss-DOX/IR780 could facilitate the accumulation of both DOX and IR780 within tumor spheroids, maximizing local drug concentration. This improved co-delivery could synergistically amplify cytotoxic effects. These results suggested that the combination of chemotherapy and phototherapy was an effective treatment strategy with potent anticancer activity.

Conclusions

In this study, a novel reduction-responsive Ser-ss-DOX has been successfully synthesized. This conjugate effectively encapsulates the photosensitizer IR780 to form Ser-ss-DOX/IR780 nanoparticles with a mean diameter of 190 nm, which remain stable under physiological conditions. Under reducing conditions, the disulfide bond of Ser-ss-DOX/IR780 nanoparticles undergoes cleavage, enabling effective drug release. The cumulative release rate of DOX from Ser-ss-DOX/IR780 nanoparticles reached ~62% in 20 mM GSH-containing PBS for 120 h. Furthermore, the Ser-ss-DOX/IR780 nanoparticles demonstrated photothermal efficacy comparable to free IR780. Ser-ss-DOX/IR780 nanoparticles exhibited high efficiency in cellular uptake and ROS generation. Notably, compared to monotherapy with either DOX or IR780, Ser-ss-DOX/IR780 nanoparticles significantly enhanced cytotoxicity against 4T1 cells. The drug-loaded nanoparticles demonstrated improved penetration within 3D tumor spheroids. Therefore, these nanoparticles exhibited potential for clinical translation. Collectively, the Ser-ss-DOX/IR780 nanoparticles represent a promising platform for combined chemo-phototherapy, and future studies will focus on the evaluation of their biosafety in vivo and efficacy against solid tumors.

Funding

This work was sponsored by the Science and Technology Plan Project of Huzhou City (2022GZ44) and the Graduate Research Innovation Project of Huzhou University (2025KYCX90).

Disclosure

The authors report no conflicts of interest in this work.

References

1. Gupta A, Jadhav SR, Colaco V, et al. Harnessing unique architecture and emerging strategies of solid lipid nanoparticles to combat colon cancer: a state-of-the-art review. *Int J Pharm*. 2025;675:125562. doi:10.1016/j.ijpharm.2025.125562
2. Ajmeera D, Ajumeera R. Drug repurposing: a novel strategy to target cancer stem cells and therapeutic resistance. *Genes Dis*. 2024;11(1):148–175. doi:10.1016/j.gendis.2022.12.013
3. Peng CM, Zheng AN, Wang LL, et al. Advances in chondroitin sulfate-based nanoplatforms for biomedical applications. *Int J Nanomedicine*. 2025;20:9857–9881. doi:10.2147/ijn.S533559
4. Wang M, Yu F, Zhang Y. Present and future of cancer nano-immunotherapy: opportunities, obstacles and challenges. *Mol Cancer*. 2025;24(1):26. doi:10.1186/s12943-024-02214-5
5. Zheng Y, Oz Y, Gu Y, et al. Rational design of polymeric micelles for targeted therapeutic delivery. *Nano Today*. 2024;55:102147. doi:10.1016/j.nantod.2024.102147
6. Farhoudi L, Hosseinikhah SM, Vahdat-Lasemi F, et al. Polymeric micelles paving the way: recent breakthroughs in camptothecin delivery for enhanced chemotherapy. *Int J Pharm*. 2024;659:124292. doi:10.1016/j.ijpharm.2024.124292
7. Gao W, Bigham A, Ghomi M, et al. Micelle-engineered nanoplatforms for precision oncology. *Chem Eng J*. 2024;495:153438. doi:10.1016/j.cej.2024.153438
8. Yu J, Wang L, Xie X, et al. Multifunctional nanoparticles codelivering doxorubicin and amorphous calcium carbonate preloaded with indocyanine green for enhanced chemo-photothermal cancer therapy. *Int J Nanomed*. 2023;18:323–337. doi:10.2147/ijn.S394896
9. Beach MA, Nayanathara U, Gao Y, et al. Polymeric nanoparticles for drug delivery. *Chem Rev*. 2024;124(9):5505–5616. doi:10.1021/acs.chemrev.3c00705
10. Hu YW, Du YZ, Liu N, et al. Selective redox-responsive drug release in tumor cells mediated by chitosan based glycolipid-like nanocarrier. *J Control Release*. 2015;206:91–100. doi:10.1016/j.jconrel.2015.03.018
11. Wei J, Qian Y, Bao L, et al. Disulfide bonds as a molecular switch of enzyme-activatable anticancer drug precise release for fluorescence imaging and enhancing tumor therapy. *Talanta*. 2024;278:126394. doi:10.1016/j.talanta.2024.126394
12. Huang H, Zhang X, Yu J, et al. Fabrication and reduction-sensitive behavior of polyion complex nano-micelles based on PEG-conjugated polymer containing disulfide bonds as a potential carrier of anti-tumor paclitaxel. *Colloids Surf B Biointerfaces*. 2013;110:59–65. doi:10.1016/j.colsurfb.2013.04.023
13. Zhang L, Hao M, Yao L, et al. Sericin "hairpin structure"-based multifunctional anthocyanin nanoencapsulation for remodeling ROS-dependent cutaneous wound healing. *Chem Eng J*. 2023;475:145863. doi:10.1016/j.cej.2023.145863
14. Wang J, Liu H, Shi XL, et al. Development and application of an advanced biomedical material-silk sericin. *Adv Mater*. 2024;36(23). doi:10.1002/adma.202311593
15. Yuan Y, Nasri M, Manayi A, et al. Sericin coats of silk fibres, a degumming waste or future material? *Mater Today Bio*. 2024;29:101306. doi:10.1016/j.mtbio.2024.101306
16. Hu D, Xu Z, Hu Z, et al. pH-triggered charge-reversal silk sericin-based nanoparticles for enhanced cellular uptake and doxorubicin delivery. *Acs Sustain Chem Eng*. 2017;5(2):1638–1647. doi:10.1021/acssuschemeng.6b02392
17. Kciuk M, Gielecińska A, Mujwar S, et al. Doxorubicin-an agent with multiple mechanisms of anticancer activity. *Cells*. 2023;12(4). doi:10.3390/cells12040659
18. Yu W, Xu H, Sun Z, et al. TBC1D15 deficiency protects against doxorubicin cardiotoxicity via inhibiting DNA-PKcs cytosolic retention and DNA damage. *Acta Pharm Sin B*. 2023;13(12):4823–4839. doi:10.1016/j.apsb.2023.09.008
19. Cui J, Chen Y, Yang Q, et al. Protosappanin a protects DOX-induced myocardial injury and cardiac dysfunction by targeting ACSL4/FTH1 axis-dependent ferroptosis. *Adv Sci*. 2024;11(34):e2310227. doi:10.1002/advs.202310227
20. Cao C, Si G, Yang N, et al. Fe^{3+}-DOX-mediated self-assembled nanolipids for tumor microenvironment activated synergistic ferroptotic-chemo therapy assisted with MR-imaging. *Sens Actuators B Chem*. 2024;415:136039. doi:10.1016/j.snb.2024.136039
21. Huang L, Tao K, Liu J, et al. Design and fabrication of multifunctional sericin nanoparticles for tumor targeting and pH-responsive subcellular delivery of cancer chemotherapy drugs. *ACS Appl Mater Interfaces*. 2016;8(10):6577–6585. doi:10.1021/acsami.5b11617
22. Jin H, Wang L, Bernards R. Rational combinations of targeted cancer therapies: background, advances and challenges. *Nat Rev Drug Discov*. 2023;22(3):213–234. doi:10.1038/s41573-022-00615-z
23. Han N, Shi Q, Wang XR, et al. Liposome co-loaded with β-elemene and IR780 for combined chemo-phototherapy. *J Drug Deliv Sci Tec*. 2022:68. doi:10.1016/j.jddst.2022.103122
24. Ruan M, Wang X, Guo M, et al. Gambogic acid and IR780 self-assembled nanoparticles for combined chemo-phototherapy. *Colloids Surf B Biointerfaces*. 2025;245:114254. doi:10.1016/j.colsurfb.2024.114254
25. Shi Z, Luo M, Huang Q, et al. NIR-dye bridged human serum albumin reassemblies for effective photothermal therapy of tumor. *Nat Commun*. 2023;14(1):6567. doi:10.1038/s41467-023-42399-9
26. Obaid G, Celli JP, Broekgaarden M, et al. Engineering photodynamics for treatment, priming and imaging. *Nat Rev Bioeng*. 2024;2(9):752–769. doi:10.1038/s44222-024-00196-z
27. Alves CG, Lima-Sousa R, de Melo-Diogo D, et al. IR780 based nanomaterials for cancer imaging and photothermal, photodynamic and combinatorial therapies. *Int J Pharm*. 2018;542(1):164–175. doi:10.1016/j.ijpharm.2018.03.020
28. Alves CG, de Melo-Diogo D, Lima-Sousa R, et al. Hyaluronic acid functionalized nanoparticles loaded with IR780 and DOX for cancer chemo-photothermal therapy. *Eur J Pharm Biopharm*. 2019;137:86–94. doi:10.1016/j.ejpb.2019.02.016
29. Pais-Silva C, de Melo-Diogo D, Correia IJ. IR780-loaded TPGS-TOS micelles for breast cancer photodynamic therapy. *Eur J Pharm Biopharm*. 2017;113:108–117. doi:10.1016/j.ejpb.2017.01.002
30. Song J, Ye H, Jiang S, et al. An acid response IR780-based targeted nanoparticle for intraoperative near-infrared fluorescence imaging of ovarian cancer. *Int J Nanomedicine*. 2022;17:4961–4974. doi:10.2147/ijn.S375145
31. Wang S, Liu Z, Tong Y, et al. Improved cancer phototheranostic efficacy of hydrophobic IR780 via parenteral route by association with tetrahedral nanostructured DNA. *J Control Release*. 2021;330:483–492. doi:10.1016/j.jconrel.2020.12.048
32. Yang J, Wang W, Huang S, et al. Production, characterization, and application of hydrophobin-based IR780 nanoparticles for targeted photothermal cancer therapy and advanced near-infrared imaging. *Adv Healthc Mater*. 2025;14(1):e2402311. doi:10.1002/adhm.202402311

33. Yu J, Zhang Y, Xu M, et al. Innovative gelatin-based micelles with AS1411 aptamer targeting and reduction responsiveness for doxorubicin delivery in tumor therapy. *Biomed Pharmacother*. 2024;174:116446. doi:10.1016/j.biopha.2024.116446
34. Yu J, Xu J, Jiang R, et al. Versatile chondroitin sulfate-based nanoplatform for chemo-photodynamic therapy against triple-negative breast cancer. *Int J Biol Macromol*. 2024;265(P1):130709. doi:10.1016/j.ijbiomac.2024.130709
35. Ren J, Liang L, Yang YQ, et al. Assembling drug-loaded-layered double hydroxide nanohybrids with poloxamer 188 for improved cellular uptake and in vitro efficacy. *J Mater Res*. 2023;38(2):337–349. doi:10.1557/s43578-022-00813-w
36. Alonezi S, Tusiimire J, Wallace J, et al. Metabolomic profiling of the synergistic effects of melittin in combination with cisplatin on ovarian cancer cells. *Metabolites*. 2017;7(2):14. doi:10.3390/metabo7020014
37. Yang X, Shi X, Zhang Y, et al. Photo-triggered self-destructive ROS-responsive nanoparticles of high paclitaxel/chlorin e6 co-loading capacity for synergetic chemo-photodynamic therapy. *J Control Release*. 2020;323:333–349. doi:10.1016/j.jconrel.2020.04.027
38. Zhang J, Zhang K, Hao Y, et al. Polydopamine nanomotors loaded indocyanine green and ferric ion for photothermal and photodynamic synergistic therapy of tumor. *J Colloid Interface Sci*. 2023;633:679–690. doi:10.1016/j.jcis.2022.11.099
39. Tian Z, Chen H, Zhao P. Compliant immune response of silk-based biomaterials broadens application in wound treatment. *Front Pharmacol*. 2025;16:1548837. doi:10.3389/fphar.2025.1548837
40. Verma J, Kanoujia J, Parashar P, et al. Wound healing applications of sericin/chitosan-capped silver nanoparticles incorporated hydrogel. *Drug Deliv Transl Res*. 2017;7(1):77–88. doi:10.1007/s13346-016-0322-y
41. Yooyod M, Ross GM, Limpeanchob N, et al. Investigation of silk sericin conformational structure for fabrication into porous scaffolds with poly (vinyl alcohol) for skin tissue reconstruction. *Eur Polym J*. 2016;81:43–52. doi:10.1016/j.eurpolymj.2016.05.023
42. Liu X, Guo Y, Wang X, et al. Preparation of cardamonin and IR780 Co-loaded on Lycium barbarum polysaccharide nanoparticles and anti-tumor efficacy evaluation. *J Drug Deliv Sci Tec*. 2024;99:106004. doi:10.1016/j.jddst.2024.106004
43. Fu S, Rempson CM, Puche V, et al. Construction of disulfide containing redox-responsive polymeric nanomedicine. *Methods*. 2022;199:67–79. doi:10.1016/j.ymeth.2021.12.011
44. Wang K, Zhang Y, Wang J, et al. Self-assembled IR780-loaded transferrin nanoparticles as an imaging, targeting and PDT/PTT agent for cancer therapy. *Sci Rep*. 2016;6(1):27421. doi:10.1038/srep27421
45. Zhang L, Shen Y, Zhang T, et al. pH responsive and zwitterionic micelle for enhanced cellular uptake and antitumor performance. *Biomater Adv*. 2025;167:214082. doi:10.1016/j.bioadv.2024.214082
46. Weng S, Pan L, Jiang D, et al. Idarubicin and IR780 co-loaded PEG-b-PTMC nanoparticle for non-Hodgkin's lymphoma therapy by photothermal/photodynamic strategy. *Mater Des*. 2023;230:112008. doi:10.1016/j.matdes.2023.112008
47. Yu J, Yuan Q, Li C, et al. Reactive oxygen species-sensitive chondroitin sulfate A-cholesteryl hemisuccinate micelles for targeted doxorubicin delivery in tumor therapy. *J Drug Deliv Sci Tec*. 2024;96:105690. doi:10.1016/j.jddst.2024.105690
48. Lopez-Vince E, Simon-Yarza T, Wilhelm C. A polysaccharide-based hydrogel platform for tumor spheroid production and anticancer drug screening. *Sci Rep*. 2025;15(1):4213. doi:10.1038/s41598-025-87896-7
49. Rodrigues DB, Reis RL, Pirraco RP. Modelling the complex nature of the tumor microenvironment: 3D tumor spheroids as an evolving tool. *J Biomed Sci*. 2024;31(1):13. doi:10.1186/s12929-024-00997-9